

Supporting Information Available for

**Halogen bond-assisted electron-transfer reactions of aliphatic
bromosubstituted electrophiles**

Sergiy V Rosokha, Michael K. Vinakos*
Department of Biological, Chemical and Physical Sciences
Roosevelt University, Chicago, IL, 60605

srosokha@roosevelt.edu

Details of the experimental measurements and computations.

Spectral measurements. UV-Vis measurements were carried out under N₂ atmosphere using quartz (1-mm or 1-cm path length) spectroscopic cells equipped with a Teflon valve fitted with Viton O-rings. A Dewar equipped with quartz lens was used for measurements at +5 to -70 °C.

[R-Br, TMPD] complex formation. The [R-Br, TMPD] formation constants and extinction coefficients were evaluated via UV-Vis titrations (by an incremental addition of R-Br to the solutions of TMPD molecules in hexane, dichloromethane or acetonitrile, see Figure 1 and Figures S1-S4 below). Spectral measurements were followed by quantitative treatment of the data using Benesi-Hildebrand method,² and via regression analysis of the UV-Vis absorbance data 1, as described earlier.^{3,4}

Specifically, the equilibrium constant for complex formation is expressed as:

$$K = x / (([R-Br] - x)([TMPD] - x))$$

where x is an equilibrium concentration of the complex and [R-Br] and [TMPD] are initial concentrations of the reactants in solution. When one of them is taken in large excess, i.e. [CBr₄] >> [TMPD], then [CBr₄] >> x , and [CBr₄] - x ≈ [CBr₄]. Therefore $K = x / ([TMPD] - x)[CBr_4]$ or $1/x = 1/[TMPD] + 1/(K [TMPD] [CBr_4])$. Taking into account that: $A = \epsilon l x$, where A is absorbance of the complex at a certain wavelength (obtained by subtraction of the absorption of components), and l is the length of the spectrophotometric cell, the latter can be rearranged as Benesi-Hildebrand equation: [1]

$$[TMPD] / A = 1/(\epsilon l) + \{1/ (K\epsilon l)\} \times 1/[CBr_4].$$

As illustrated for the CBr₄/TMPD and CBr₃NO₂/TMPD pairs in Figures S1 and S3, the plot [TMPD] / A vs 1/[R-Br] is described by a linear trend line, which produces values of K and ϵ in Table S1.

Table S1. Spectral and thermodynamic characteristic of the [R-Br, TMPD] complexes

Complex	Solvent	λ_{max} , nm	ϵ , M ⁻¹ cm ⁻¹	K , M ⁻¹
[CBr ₄ , TMPD]	C ₆ H ₁₄	370	4.0	0.4
[CBr ₄ , TMPD]	CH ₂ Cl ₂	380	3.2	0.3
[CBr ₄ , TMPD]	CH ₃ CN	374	2.5	0.4
[CBr ₃ NO ₂ , TMPD]	C ₆ H ₁₄	360	3.3	1.2
[CBr ₃ NO ₂ , TMPD]	CH ₂ Cl ₂	360	-	-

It should be noted that the Benesi-Hildebrand procedure provided reliable results only if one reactant is present in large excess and the complexation of the other reactant (in deficit) is in the 20-80% range⁵ (which is difficult to obtain if the K values of ~ 1 or less). Thus, to verify the values of K and ϵ , we

carried out regression analysis of the absorbances of complexes at various concentrations of the components (similar to that described earlier^{3,4}), without the assumption made in the Benesi-Hildebrand method. In this case, the expression for the equilibrium constant, $K = x/([R-Br] - x)([TMPD] - x)$, leads to the quadratic equation: $x^2 - x([R-Br] + [TMPD] + 1/K) + [R-Br][TMPD] = 0$. The physically meaningful solution of this equation is:

$$x = ([R-Br] + [TMPD] + 1/K)/2 - \{([R-Br] + [TMPD] + 1/K)^2 - 4[R-Br][TMPD]\}^{1/2}/2$$

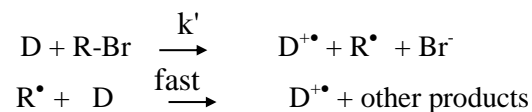
Accordingly, the absorbance of the complex can be calculated as:

$$A_{\text{calc}} = \varepsilon l \{([R-Br] + [TMPD] + 1/K)/2 - \{([R-Br] + [TMPD] + 1/K)^2 - 4[R-Br][TMPD]\}^{1/2}/2\}$$

Computer fitting of the series of experimental values of absorption A_{exp}^i measured at different initial concentrations of R-Br and TMPD (by the variation of ε and K values to minimize the difference between the experimental and calculated values of the absorption: $\Delta = \sum \{A_{\text{exp}}^i - A_{\text{calc}}^i\}^2$ and to maximize the correlation coefficient between A_{exp}^i and A_{calc}^i values) produced a unitary set of K and ε which describes the absorption of the complex over a wide range of concentrations of components.

3-4 series of experiments were performed for each R-Br/TMPD pair, and values of K were evaluated at two wavelengths. Values of K obtained from different series of measurements via different methods and different wavelengths were typically within ~30 %.

Kinetics of R-Br/TMPD reactions. Addition of R-Br electrophiles to the solutions of TMPD or Fc* in dichloromethane or acetonitrile resulted in the formation of the corresponding cation-radicals $\text{TMPD}^{+\bullet}$ and $\text{Fc}^{*\bullet}$, as indicated by the appearance of the characteristic absorption bands of the latter (Figure 3 and Figure S7). For all redox-pairs, the rate constants in Table 1 were established from the studies of the initial rates of the reactions, which were proportional to the first order of concentrations of the reactants (Figure S6). It should be noted that under the conditions of experiments, two moles of the cation radical were formed per one mole CBr_3NO_2 (within 15% accuracy). For such processes, the kinetic curve could be simulated up to ~90% conversion based on the reaction scheme in which oxidation of D by R-Br electrophile resulting in formation of R^\bullet and Br^- followed by the fast oxidation of the second molecule of D by R^\bullet (or a product of their recombination), i.e.



where $k' = 1/2 k^{\text{obs}}$ (Figure S5). The equilibrium (final) concentrations of $\text{TMPD}^{+\bullet}$ cation radicals in similar reactions with CBr_4 were 5-25% of the initial concentration of TMPD (even in solutions with excess of CBr_4), indicating the significance of back reactions and/or $\text{TMPD}^{+\bullet}$ decomposition in these systems.

Computations of the outer-sphere ET rate constants. Rate constants for the outer-sphere

(intermolecular) ET processes are evaluated as:⁶ $k_{ET}^{OS} = Z \exp(-\Delta G^*/RT)$,

where $Z = 10^{11} M^{-1} s^{-1}$ is a collision factor⁷ and ΔG^* is an activation barrier.

Details of the calculation of the outer-sphere rate constants k_{ET}^{OS} are listed in Table S2.

Table S2. Parameters for the calculations of outer-sphere ET rate constants (CH₃CN, 22 °C).

Redox pair	ΔG^o , ^a kcal M ⁻¹	λ_s , ^b kcal M ⁻¹	λ , ^c kcal M ⁻¹	ΔG^*_{OS} , ^d kcal M ⁻¹	k_{ET}^{OS} , M ⁻¹ s ⁻¹
TMPD/CBr ₃ NO ₂	11.3	20.2	71.9	22.3	3.7×10^{-6}
Fc* /CBr ₃ NO ₂	6.0	18.7	58.4	16.2	0.12
TMPD/CBr ₄	13.9	20.3	82.0	27.0	1.4×10^{-9}
Fc*/CBr ₄	8.6	18.8	68.6	20.8	4.9×10^{-5}

a) Calculated as $\Delta G^o = -F\Delta E$, where F is a Faraday constant, oxidation potentials of TMPD and Fc* are 0.10 V and -0.13 V vs SCE, respectively,⁷ and reduction potentials of CBr₄ and CBr₃NO₂ are -0.50 V and -0.39 V vs SCE, respectively. Note that the reduction potentials for CBr₄ and CBr₃NO₂ (in which electron transfer occur via concerted dissociative mechanism, as indicated by quantum-mechanical computations and CV measurements) were calculated according to the methods available in the literature^{9,10} as described below.

b) The solvent reorganization energy calculated from the two-sphere Marcus expression as:⁶

$$\lambda_s = (1/\epsilon_\infty - 1/\epsilon_0) \times (\Delta q)^2 (1/2r_D + 1/2r_A - 1/r_{DA})$$

where ϵ_∞ and ϵ_0 are optical and static dielectric constants of acetonitrile, Δq is the transferred charge, r_D and r_A are effective molecular radii of the donor and acceptor, and r_{DA} is donor / acceptor separation. The effective radii of the donors and acceptors are: $r(\text{TMPD}) = 4.62 \text{ \AA}$, $r(\text{Fc}^*) = 5.90 \text{ \AA}$, $r(\text{CBr}_4) = 4.05 \text{ \AA}$, $r(\text{CBr}_3\text{NO}_2) = 4.06 \text{ \AA}$. These values were calculated from the molecular volume of the corresponding species obtained via B3LYP/6-311G* calculations, as described earlier.⁹

c) Reorganization energy calculated for the “sticky” dissociative ET mechanism,⁸ as:

$$\lambda = \lambda_i + \lambda_s + (D_{RBr}^{1/2} - D_{R\bullet/Br^-}^{1/2})^2$$

where λ_i is an intramolecular reorganization energy of the electron donors: $\lambda_i(\text{TMPD}) =$; ¹¹ D_{RBr} is the C-Br bond dissociation energy of R-Br molecules calculated according to the literature¹² (vide infra): $D_{RBr}(\text{CBr}_4) = 58.69 \text{ kcal/mol}$ and $D_{RBr}(\text{CBr}_3\text{NO}_2) = 56.76 \text{ kcal/mol}$; $D_{R\bullet/Br^-}$ is an interaction energy in the R^\bullet/Br^- radical/ion pair resulting from the dissociation of $R-Br^\bullet$ anion-radical (obtained, as described below, via ω B97XD/6-311+G(d,p) computations which were found to be in agreement with experimental enthalpies³: $D_{R\bullet/Br^-}(\text{CBr}_4) = 0.42 \text{ kcal/mol}$ and $D_{R\bullet/Br^-}(\text{CBr}_3\text{NO}_2) = 1.64 \text{ kcal/mol}$.

d) Activation barrier for the “sticky” dissociative ET mechanism the latter is calculated as:

$$\Delta G^* = \lambda/4 \{ 1 + (\Delta G^o + w_p - D_{R\bullet/Br^-})/\lambda \}^2$$

where w_p is the work of bringing products together calculated as an energy of electrostatic interaction between ionic products of the redox reactions in acetonitrile (i.e., $e^2/\epsilon r$) based on the effective molecular radii of cations and van der Waals radius of bromide of 1.85 Å: $w_p(\text{TMPD}^+/\text{Br}^-) = 1.43 \text{ kcal/mol}$, and $w_p(\text{Fc}^{*\cdot}/\text{Br}^-) = 1.19 \text{ kcal/mol}$.

Computations of the (inner-sphere) ET rate constants via [R-Br, TMPD] intermediate. According to the two-state model, the ground- and excited-state wavefunctions for the ET system consist of linear combinations of the initial (D/A) and the final (D^+/A^-) states expressed as ψ_a and ψ_b :^{9,13}

$$\Psi_{GS} = a \psi_a + b \psi_b$$

$$\Psi_{ES} = a' \psi_a + b' \psi_b$$

The solution of the secular determinant leads to the ground-state and excited-state energies as:

$$E_{GS} = (H_{aa} + H_{bb})/2 - ((H_{bb} - H_{aa})^2 + 4H_{ab}^2)^{1/2}/2 \quad (\text{A})$$

$$E_{ES} = (H_{aa} + H_{bb})/2 + ((H_{bb} - H_{aa})^2 + 4H_{ab}^2)^{1/2}/2 \quad (\text{B})$$

where $H_{aa} = \int \psi_a H \psi_a$ and $H_{bb} = \int \psi_b H \psi_b$ represent the energies of the initial and final diabatic states and $H_{ab} = \int \psi_a H \psi_b$ is the electronic coupling element. The energies of the initial and final diabatic states can be expressed at each point (X) along the reaction coordinate via the reorganization energy (λ) and the free-energy change (ΔG_{ET}^0) as: $H_{aa} = \lambda X^2$ and $H_{bb} = \Delta G_{ET}^0 + \lambda(X-1)^2$. The electronic coupling element is evaluated from the intensity integral of the absorption via the Hush expression:

$$H_{ab} = 0.0206(\nu_{CT} \Delta\nu_{1/2} \epsilon_{CT})^{1/2}/r_{DA}$$

where ν_{CT} and $\Delta\nu_{1/2}$ are the spectral maximum and full-width at half maximum (cm^{-1}), respectively, of the charge-transfer absorption band, ϵ_{CT} is the extinction coefficient ($\text{M}^{-1}\text{cm}^{-1}$), and r_{DA} (\AA) is the separation parameter. The interaction of the initial and final diabatic states (which is essentially equivalent to the donor/acceptor coupling) results in the formation of the adiabatic ground state and the excited state for the electron transfer described by the wavefunctions above. Accordingly, adiabatic ground and excited state energies can be calculated at each point of the reaction coordinate from $X = 0$ (corresponding to the neutral donor/acceptor dyad) to $X = 1$ (corresponding to the ion-radical pair) using energies of the diabatic states (i.e. $H_{aa} = \lambda X^2$, $H_{bb} = \Delta G_{ET}^0 + \lambda(X-1)^2$) and a constant value of H_{ab} (determined via the Hush formalism) via eqs (A) and (B) above. Such adiabatic ground-state diagram for electron transfer in the TMPD/CBr₄ pair is illustrated in Figure 4. Parameters, which were used in the computations of the ET energy diagrams, as well as details of the computations of the inner-sphere ET for the TMPD/CBr₄ and TMPD/CBr₃NO₂ pairs are listed in Table S3.

TableS3. Characteristics of the inner-sphere ET reactions

Redox pair	$\lambda_s(\text{IS})^a$ kcal M ⁻¹	λ_{IS}^b kcal M ⁻¹	H_{ab}^c kcal M ⁻¹	$\Delta G^*_{\text{IS}}^d$ kcal M ⁻¹	k_{ET}^e s ⁻¹	K^f M ⁻¹	$k_{\text{ET}}^{\text{IS}b}$ M ⁻¹ s ⁻¹
TMPD/CBr ₄	17.7	79.4	7.1	21.0	3.6×10 ⁻⁴	0.4	1.4×10 ⁻⁴
TMPD/CBr ₃ NO ₂	15.3	66.9	7.3	16.4	0.85	1.2	1.0

- a) Due to the close contact of the donor and acceptor in the precursor complex, Marcus (two-sphere) model is not suitable for the calculation of the solvation reorganization energy. As such, the solvation component of the reorganization energy was calculated within the framework of the dielectric continuum model (DCM) as the free energy of the inertial solvent response to a charge shift in the solute cavity:¹⁴

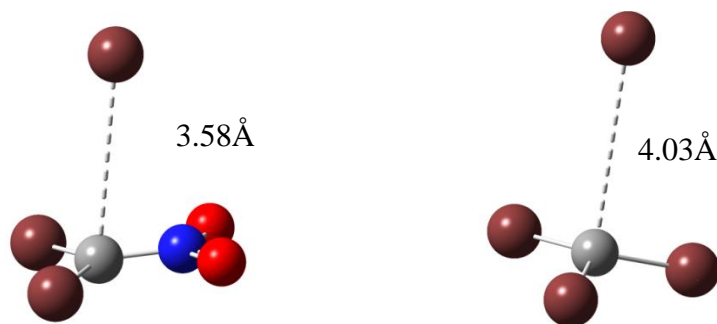
$$\lambda_s = G_s(\epsilon_{\infty 1}, \epsilon_{\infty 2}, \dots, \epsilon_{\infty N}, \Delta \mathbf{q}) - G_s(\epsilon_{01}, \epsilon_{02}, \dots, \epsilon_{0N}, \Delta \mathbf{q})$$

where $\Delta \mathbf{q}$ is the point-charge representation of the full shift in the charge density of the donor/acceptor dyad upon electron transfer. Thus the limiting Marcus two-sphere model (TSM) for the reorganization energy λ_o in bimolecular ET (vide supra) is replaced by the general approach in which the more realistic dielectric continuum framework is based on the full solution of the Poisson equation for the solute cavity of a given size, shape, and charge distribution immersed in a solvent environment. For the cavity containing the precursor complex, the change in charge density is represented by the variation of the point charge (Δq_i) at each atomic site (i). In other words, this equation represents the outer-shell reorganization energy λ_s as the free energy of the inertial solvent response to a solute with charge density $\Delta \mathbf{q}$. This solvent inertial response involves solvent nuclear polarization modes and is calculated as the difference between the optical response and the full response given as the first and the second term, respectively. [Such a difference is also implicit in the classical Marcus two-sphere model in which the solvation energies, G_s and λ_o are quadratic functions of Δq_i when the solute is linearly coupled to the solvent medium.] The reorganization energies λ_s for [TMPD,CBr₄] and [TMPD,CBr₃NO₂] complexes were calculated using the Delphi Poisson solver.¹⁵ The Δq_i values were evaluated as the difference between corresponding ESP atomic charges calculated for the isolated neutral donor and acceptor molecules and their ion-radicals. These ESP charges (as fitted to reproduce the electrostatic potential due to the solute in its immediate environment), were obtained with the aid of the ChelpG option in B3LYP/6-311G(d) calculations. The geometries of the complexes were based on their X-ray crystal structures. Comparison with the values of λ_s in Table S2, indicates that such a model produces solvent reorganization energies about 20 % lower than those resulting from the Marcus (two-sphere) expression.

- b) Calculated as described above for outer-sphere ET in Table S2, with λ_s replaced with $\lambda_s(\text{IS})$.
- c) $H_{\text{ab}} = 0.0206(v_{\text{CT}} \Delta v_{1/2} \epsilon_{\text{CT}})^{1/2} / r_{\text{DA}}$.
 [TMPD, CBr₄]: $v_{\text{CT}} = 26.7 \times 10^3 \text{ cm}^{-1}$, $\Delta v_{1/2} = 7.0 \times 10^3 \text{ cm}^{-1}$, $\epsilon_{\text{CT}} = 3200 \text{ M}^{-1} \text{ cm}^{-1}$, $r_{\text{DA}} = 6.4 \text{ \AA}$.
 [TMPD, CBr₃NO₂]: $v_{\text{CT}} = 27.8 \times 10^3 \text{ cm}^{-1}$, $\Delta v_{1/2} = 7.0 \times 10^3 \text{ cm}^{-1}$, $\epsilon_{\text{CT}} = 3300 \text{ M}^{-1} \text{ cm}^{-1}$, $r_{\text{DA}} = 6.5 \text{ \AA}$.
 (Note that since UV-Vis studies revealed minor variation of the spectral characteristics of the [R-Br, TMPD] complexes with solvent (Table S1), H_{ab} values for the [TMPD, CBr₃NO₂] complex were evaluated based on its characteristics in hexane).
- d) ΔG^*_{IS} was evaluated graphically, or alternatively, via accurate expression derived by Sutin and Brunschwig for the unsymmetric adiabatic systems with non-negligible H_{ab} in ref 13b:
 $\Delta G^* = \lambda/4 + \Delta G^o/2 + (\Delta G^o)^2/(4(\lambda - 2H_{\text{ab}})) - H_{\text{ab}} + H_{\text{ab}}^2/(\lambda + \Delta G^o) - H_{\text{ab}}^4 \Delta G^o/(\lambda + \Delta G_T)^2$
- e) Intra-molecular rate constant calculated, as described earlier for the π -bonded complexes,¹⁰ as $k_{\text{ET}} = \kappa_{\text{el}} v_n \exp(-\Delta G^*/RT)$, where $\kappa_{\text{el}} v_n \sim 10^{12} \text{ s}^{-1}$.
- f) Complex formation constant.
- g) Second-order rate constant calculated as $k_{\text{ET}}^{\text{IS}} = K k_{\text{ET}}$ (which is valid for the reactions that are significantly slower than the diffusion rates).

Computations. Quantum-mechanical calculations were carried out using the Gaussian 09 programs.¹⁶

Evaluation of interaction in $\text{CBr}_2\text{NO}_2\cdot\text{Br}^-$ and $\text{CBr}_3\cdot\text{Br}^-$ radical/ion pairs. Since $\omega\text{B97XD}/6\text{-}311+\text{G}(\text{dp})$ computations produced structures and energies of the halogen bonded complexes, which agreed well with the experimental data,³ we used this method for evaluation of $\text{CBr}_2\text{NO}_2\cdot\text{Br}^-$ (left) and $\text{CBr}_3\cdot\text{Br}^-$ radical/ion pairs. Equilibrium structures of $\text{CBr}_2\text{NO}_2\cdot\text{Br}^-$ (left) and $\text{CBr}_3\cdot\text{Br}^-$ radical/ion pairs resulting from $\omega\text{B97XD}/6\text{-}311+\text{G}(\text{dp})$ optimization of $\text{CBr}_3\text{NO}_2\cdot$ and $\text{CBr}_4\cdot$ in acetonitrile are illustrated below, and their energetics are summarized in Table S4. NBO analysis produced charges residing on bromine fragment of -0.970 and -0.995 for $\text{CBr}_2\text{NO}_2\cdot\text{Br}^-$ and $\text{CBr}_3\cdot\text{Br}^-$ pairs, respectively (Mulliken charges are practically the same for both pairs).



Atomic coordinates

$\text{CBr}_3\cdot\text{Br}^-$				$\text{CBr}_2\text{NO}_2\cdot\text{Br}$			
C	0.77269900	0.00174100	-0.00255300	C	0.84211900	0.00015200	0.30685600
Br	1.07426800	-1.83696300	0.18160900	Br	1.20741800	-1.60125000	-0.50960500
Br	0.99635500	0.76360800	-1.69790400	Br	1.20570300	1.60213200	-0.50922300
Br	1.05375300	1.09198600	1.49323100	Br	-2.67938100	-0.00062400	-0.35629300
Br	-3.25683800	-0.01893000	0.02350100	N	0.32651700	-0.00032000	1.64292500
				O	0.12372400	-1.08370500	2.17384200
				O	0.12387000	1.08274100	2.17461000

Table S4. Summary of the $\omega\text{B97XD}/6\text{-}311+\text{G}(\text{dp})$ computations of $\text{R}\cdot/\text{Br}^-$ interaction enthalpy in CH_3CN

	E, Eh	H, Eh	BSSE, Eh	ΔH , kcal/mol
Br^-	-2574.362917	-2574.360557		
$\text{CBr}_2\text{NO}_2\cdot\text{Br}^-$	-7965.843965	-7965.816016	0.000353021	-1.65
$\text{CBr}_2\text{NO}_2\cdot$	-5391.477571	-5391.452482		
$\text{CBr}_3\cdot\text{Br}^-$	-10334.91777	-10334.90323	0.000152734	-0.43
$\text{CBr}_3\cdot$	-7760.553541	-7760.541839		

Computations of the bond dissociation energy of CBr₄ and CBr₃NO₂. Bond dissociation energies for the R-Br molecules were calculated as described by Lin, Coote, Gennaro and Matyjaszewski in ref. 12 using a high-level composite G3(MP2)-RAD(+) method that approximate (UR)CCSD(T) energies with a large triple basis set via additivity corrections at the R(O)MP2 level of theory. The results of these computations are summarized in Table S5.

Atomic coordinates:

CBr ₄				CBr ₃ [•]			
C	-0.00013300	0.00007300	-0.00002600	C	0.00012000	0.00000200	0.34054900
Br	-1.85625800	-0.08115400	-0.59191400	Br	1.81398900	0.37801900	-0.01946300
Br	0.42419000	1.81837800	0.56166900	Br	-0.57959400	-1.75979500	-0.01945900
Br	1.17395700	-0.51706400	-1.46841400	Br	-1.23441600	1.38177700	-0.01945800
Br	0.25813400	-1.22017200	1.49866300				
CBr ₃ NO ₂				CBr ₂ NO ₂ [•]			
C	-0.00001900	-0.01507500	0.12480600	C	-0.00000300	0.20530900	-0.00006700
Br	1.58644500	-0.99312800	-0.35159600	Br	1.60733200	-0.68753100	0.00001400
Br	0.00078200	1.75778700	-0.67066900	Br	-1.60732600	-0.68754000	-0.00000300
Br	-1.58736800	-0.99168900	-0.35157300	N	-0.00000200	1.64870700	-0.00007800
N	0.00016700	0.26464200	1.69606600	O	1.10142600	2.20967500	-0.00001800
O	-1.09178100	0.38661800	2.21657200	O	-1.10144800	2.20966000	0.00008900
O	1.09226900	0.38638400	2.21630600				

Table S5. Summary of the computations of bond dissociation energies of R-Br electrophile.

	E, Eh ^a	H, Eh	BDE, kcal/mol ^b
Br [•]	-2572.825969	-2572.823609	
CBr ₂ NO ₂ [•]	-5388.602922	-5388.595928	
CBr ₃ NO ₂	-7961.518971	-7961.510006	56.77
CBr ₃ [•]	-7756.597477	-7756.591346	
CBr ₄	-10329.51626	-10329.50849	58.69

a) $E(\text{G3(MP2)-RAD}) = E[\text{MP2/G3MP2Large}] + \Delta\text{EC}[\text{CCSD(T)/6-31G(d)}] + \text{HLC} + \text{ZPVE} + E[\text{SO}]$
 $E[\text{MP2/G3MP2Large}]$ is the the MP2/G3MP2Large total energy.

$\Delta\text{EC}[\text{CCSD(T)/6-31G(d)}] = E[\text{CCSD(T)/6-31G(d)}] - E[\text{MP2/6-31G(d)}]$

HLC is a correction term that depends on the number of α and β valence electrons ($n\alpha$ and $n\beta$).

It is obtained with parameters A, B, C and D as:

$\text{HLC} = -A n\beta - B (n\alpha - n\beta)$ for molecules and $\text{HLC} = -C n\beta - D (n\alpha - n\beta)$ for atomic species

where $A = 9.413$, $B = 3.969$, $C = 9.438$, $D = 1.888$ (in mHartree)

Scaled B3LYP/6-31G(d) frequencies (0.9806) are used to obtain the ZPVE and thermal corrections to enthalpy. A spin-orbit correction, i.e., $E[\text{SO}]$, where available from experimental data or from accurate calculations, is included.

b) $\text{BDE} = -[\text{H(R-Br)} - \text{H(R)} - \text{H(Br)}]$. Note that experimental value of BDE for CBr₄ is 57.91 kcal/mol.

Computations of reduction potentials of R-Br molecules in acetonitrile. Reduction potentials of the R-Br molecules in acetonitrile, $R-X_s + e^- \rightarrow R^{\bullet}_s + X^-_s$ were calculated as described by Isse, Lin, Coote and Gennaro in ref. 17 as a sum of the Gibbs free energies of the reactions $R-X_s \rightarrow R^{\bullet}_s + X^{\bullet}_s$ and $X^{\bullet}_s + e^- \rightarrow X^-_s$. The free energy of the first reaction can be estimated using the free energy of the same reaction in the gas phase (obtained from the G3(MP2)-RAD(+) computations described in the previous section) and the free energies of solvation. Solvation energies were calculated, as in ref. 17, using the conductor-like polarizable continuum model, CPCM, level for the structures optimized at HF/6-31+G(d) level with UAHF radii. The results of these computations are summarized in Table S6.

Table S6. Summary of the computations of the reduction potentials of R-Br molecules.

	$G_{\text{gas}}, \text{Eh}^a$	$G_{\text{AN}}, \text{Eh}^a$	$G_{\text{solv}}, ^b$ kcal/mol	$\Delta\Delta G_{\text{solv}}, ^c$ kcal/mol	BDE, ^d kcal/mol	TΔS, ^e kcal/mol	$E_{\text{red}}^{\circ}, \text{V}^f$ vs SCE ^a
Br	-2569.893258	-2569.89468	-0.89				
CBr ₂ NO ₂	-5381.673283	-5381.681678	-5.27				
CBr ₃ NO ₂	-7951.60471	-7951.611236	-4.10	-2.06	56.77	8.83	-0.39
CBr ₃	-7747.539831	-7747.541883	-1.29				
CBr ₄	-10317.47612	-10317.47895	-1.78	-0.40	58.69	9.81	-0.51 ^g

a) G_{AN} and G_{gas} were calculated at ROHF/6-31+G(d) level of theory in gas phase and in acetonitrile (with `scrf=(cpcm, solvent=acetonitrile)` option) for species obtained by optimization at hf/6-31+g(d) level in acetonitrile (`scrf=(cpcm, solvent=acetonitrile)`)

b) $G_{\text{solv}} = G_{\text{AN}} - G_{\text{gas}}$

c) $\Delta\Delta G_{\text{solv}} = G_{\text{solv}}(\text{R}) + G_{\text{solv}}(\text{Br}) - G_{\text{solv}}(\text{R-Br})$

d) See Table S5

e) Calculated as difference in entropies obtained via G3(MP2)-RAD(+) method.

f) $E_{\text{red}}^{\circ} = 1/F \times (-\text{BDE} + \text{T}\Delta\text{S} - \Delta\Delta G_{\text{solv}}) + 1.60$, where 1.60 is a reduction potential of the bromine atom in acetonitrile.¹⁷

g) Note that ref. 17 reports a slightly different value of the reduction potential of CBr₄ (-0.48 V vs SCE). The 0.03 V difference is related to the fact that calculations of the reduction potential of CBr₄ in ref 17 were based on the TΔS and ΔΔG_{solv} taken as the average values of the corresponding parameters for the series of R-Br molecules calculated in ref. 12 (which did not include CBr₄). In comparison, we calculated these values specifically for CBr₄ (and CBr₃NO₂) according to the methodology described in ref. 12.

Reduction potentials of R• radicals in acetonitrile were calculated as described in ref. 12 based on the Gibbs free energy of the reactions $R_s^\bullet + e^- \rightarrow R_s^-$. The results of computations are summarized in Table S7.

Table S7. Summary of computations of the reduction potentials of R• radicals in acetonitrile.

	G_{AN} , Eh ^a	G_{gas} , Eh ^a	$\Delta\Delta G_{solv}$, ^b kcal/mol	H_{gas} , Eh ^c	S_{gas} , ^c kcal / mol	ΔG_{gas} ^d kcal/mol	ΔG_{AN} ^e kcal/mol	E_{red}^o , ^f V vs SCE ^a
CBr_2NO_2	-5381.681678	-5381.67328	-50.95	-5388.595928	85.33	-67.66	-118.61	0.76
$CBr_2NO_2^-$	-5381.840603	-5381.75101		-5388.704552	83.65			
CBr_3	-7747.541883	-7747.53983	-46.98	-7756.591346	82.81	-56.92	-103.89	0.12
CBr_3^-	-7747.67105	-7747.59413		-7756.681748	83.42			

- G_{AN} and G_{gas} were calculated at ROHF/6-31+G(d) level of theory in gas phase and in acetonitrile (with scrf=(cpcm, solvent=acetonitrile) option) for species obtained by optimization at HF/6-31+g(d) level in acetonitrile (scrf=(cpcm, solvent=acetonitrile))
- $\Delta\Delta G_{solv} = (G_{solv}(R^-) - G_{solv}(R))$ where $G_{solv}(X) = G_{AN}(X) - G_{gas}(X)$;
- $\Delta H_{gas} = H(R^-) - H(R)$ and $\Delta S = S(R^-) - S(R)$, where H and S were calculated at G3(MP2)-RAD level
- $\Delta G_{gas} = \Delta H_{gas} - T\Delta S$
- $\Delta G_{AN} = \Delta G_{gas} + \Delta\Delta G_{solv}$
- $E_{red}^o = -\Delta G_{AN}/F - 4.388$, where 4.388 V is obtained by adding the SCE potential (0.241 V) to the absolute SHE potential (4.24 V) and subtracting interliquid potential (0.093 V).

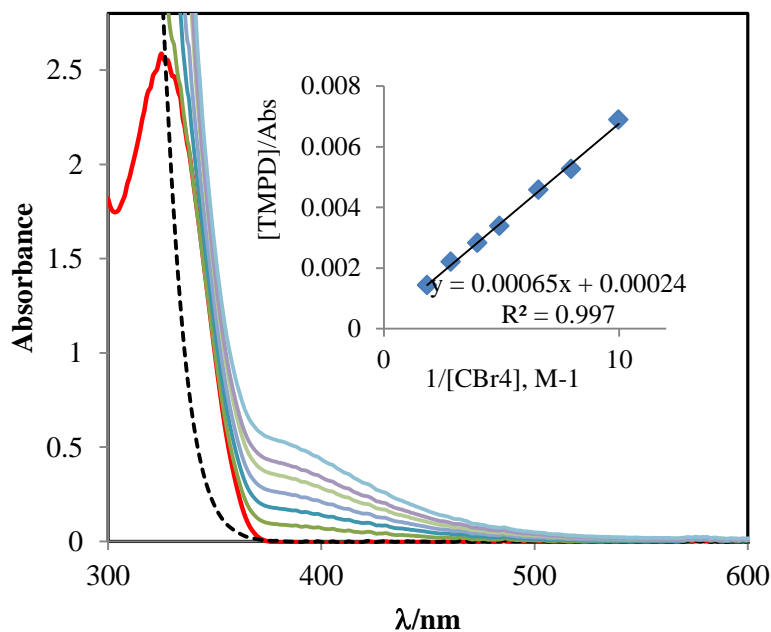


Figure S1. Spectra of hexane solutions of TMPD (1 mM) together with 0, 0.052, 0.10, 0.15, 0.20, 0.25 and 0.35 M of CBr_4 (solid lines from the bottom to the top); dashed line: spectrum of separate 0.25 M solution of CBr_4 (22°C , $l = 1\text{ cm}$). Insert: Benesi-Hildebrand treatment of spectral data leading to extinction coefficient of $\varepsilon = 4 \times 10^3\text{ M}^{-1}\text{ cm}^{-1}$ and formation constant $K = 0.4\text{ M}^{-1}$ for $[\text{CBr}_4, \text{TMPD}]$ complex.

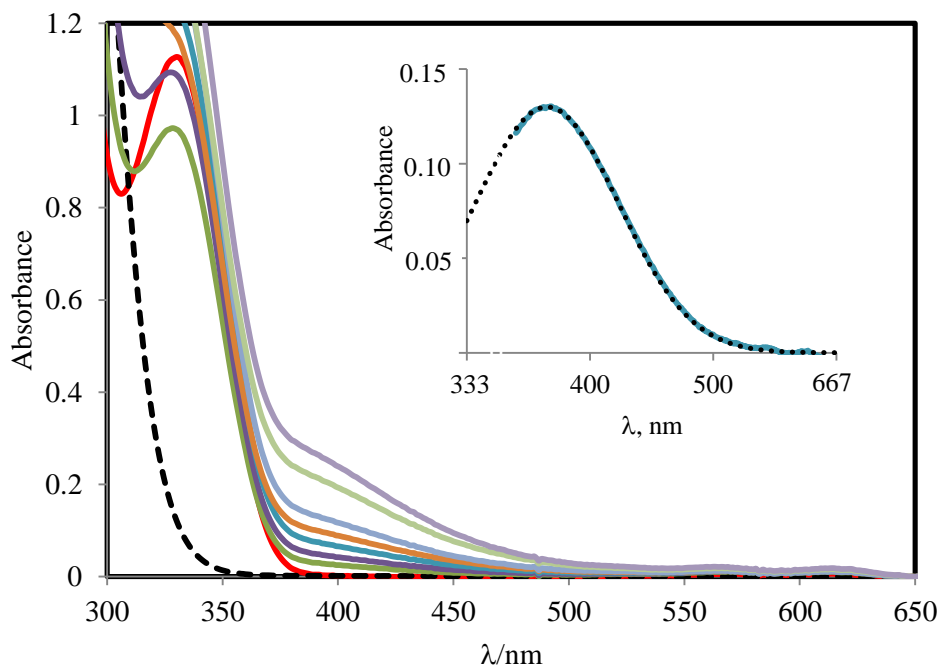


Figure S2. Spectra of acetonitrile solutions of TMPD (4.9 mM) measured immediately after mixing with 0, 0.05, 0.10, 0.15, 0.20, 0.25, 0.40 and 0.50 M of CBr_4 (solid lines from the bottom to the top); dashed line: spectrum of separate 0.25 M solution of CBr_4 (22°C , $l = 0.1\text{ cm}$). Insert: Gaussian fitting (dotted line) of the absorption band of $[\text{CBr}_4, \text{TMPD}]$ complex obtained by the subtraction of the absorptions of TMPD and CBr_4 components from the absorption of their mixture in acetonitrile.

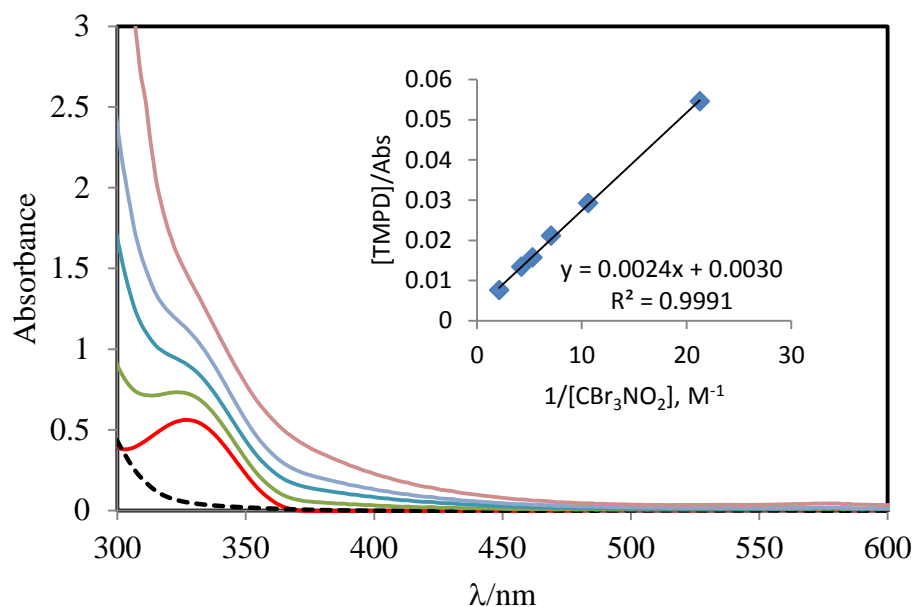


Figure S3. Spectra of hexane solutions of TMPD (2.4 mM) together with 0, 0.047, 0.141, 0.235, and 0.47 M of CBr_3NO_2 (solid lines from the bottom to the top); dashed line: spectrum of separate 0.25 M solution of CBr_4 (22° C, $l=0.1$ cm). Insert: Benesi-Hildebrand treatment of spectral data leading to extinction coefficient of $\epsilon = 3.3 \times 10^3 \text{ M}^{-1} \text{ cm}^{-1}$ and formation constant $K = 1.2 \text{ M}^{-1}$ for $[\text{CBr}_4, \text{TMPD}]$ complex.

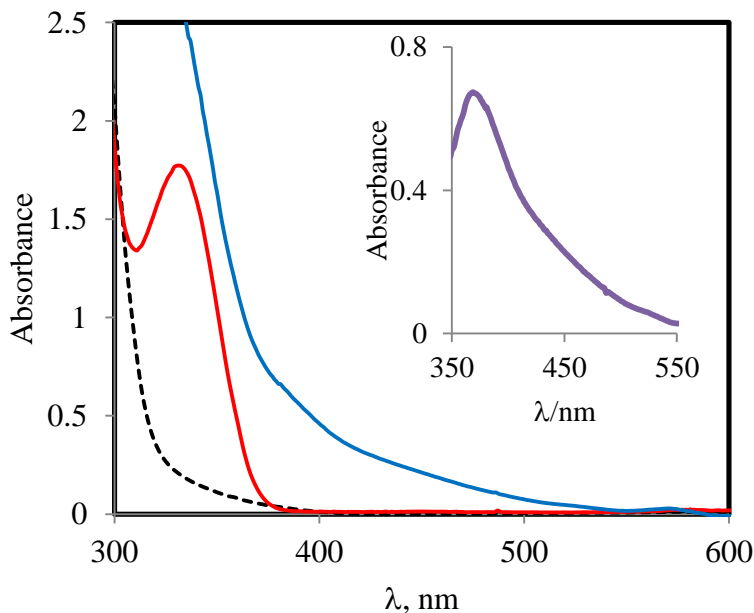


Figure S4. Spectrum of the mixture of TMPD (2 mM) and CBr_3NO_2 (2mM) measured at -80°C in dichloromethane (blue line) together with the spectra of separate 2 mM solutions of TMPD (red line) and CBr_3NO_2 (dashed line) ($l=1$ cm). Insert: Absorption of $[\text{CBr}_3\text{NO}_2, \text{TMPD}]$ complex obtained by the subtraction of the absorptions of TMPD and CBr_3NO_2 components from the absorption of their mixture.

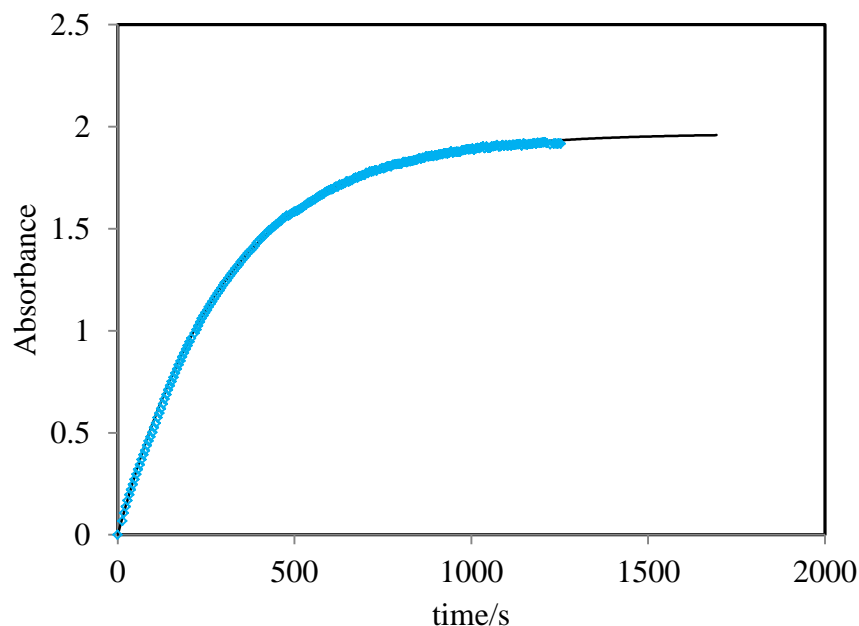


Figure S5. Changes of the intensity of absorbance at 611 nm (corresponding to $\text{TMPD}^{\bullet+}$ cation radical) upon addition of CBr_3NO_2 (0.86 mM) to the 10 mM solution of TMPD in dichloromethane. Black line represents kinetic curve calculated as $\text{Abs} = \epsilon l \times [\text{TMPD}^{\bullet+}]$, where ϵ its extinction coefficient of $\text{TMPD}^{\bullet+}$ at 611 nm, l is length of the spectrophotometric cell and $[\text{TMPD}^{\bullet+}]$ is a concentration of the product calculated assuming fast oxidation of the second molecule of TMPD by $\text{CBr}_2\text{NO}_2^{\bullet}$ radical as: $[\text{TMPD}^{\bullet+}] = 2ab(e^{akt} - e^{2bkt}) / (ae^{akt} - 2be^{2bkt})$, where a is initial concentration of TMPD and b is initial concentration of CBr_3NO_2 , and $k = 1/2 k^{obs}$.

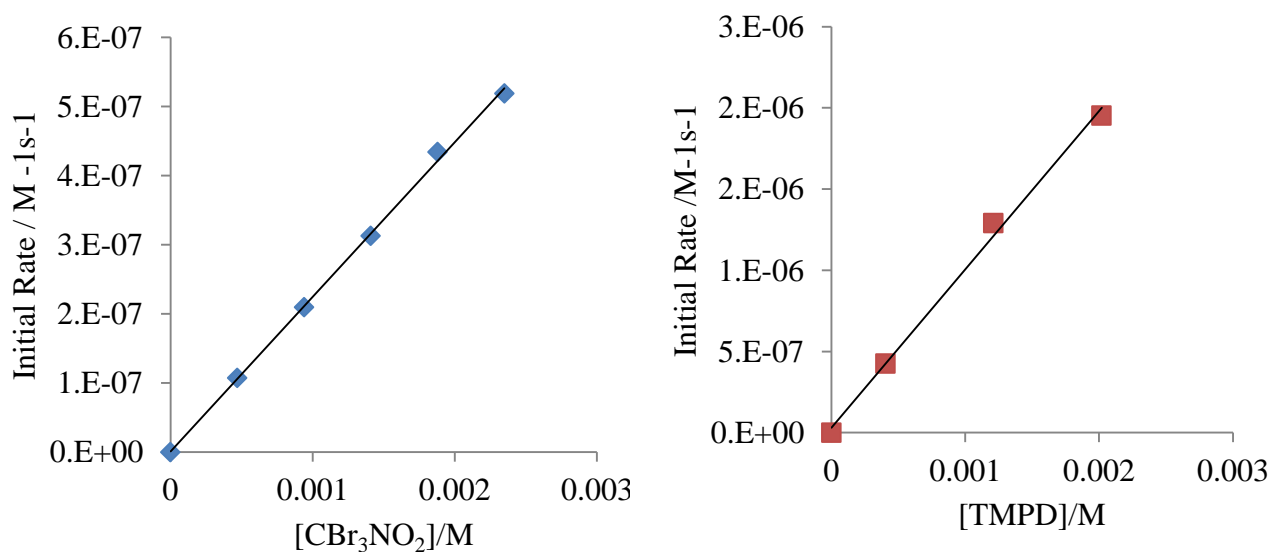


Figure S6. Linear dependences of the initial rates of the oxidation of TMPD by CBr_3NO_2 in dichloromethane on concentration of CBr_3NO_2 (at $[\text{TMPD}]_0 = 0.43\text{mM}$) and $[\text{TMPD}]$ (at $[\text{CBr}_3\text{NO}_2]_0 = 1.9\text{mM}$).

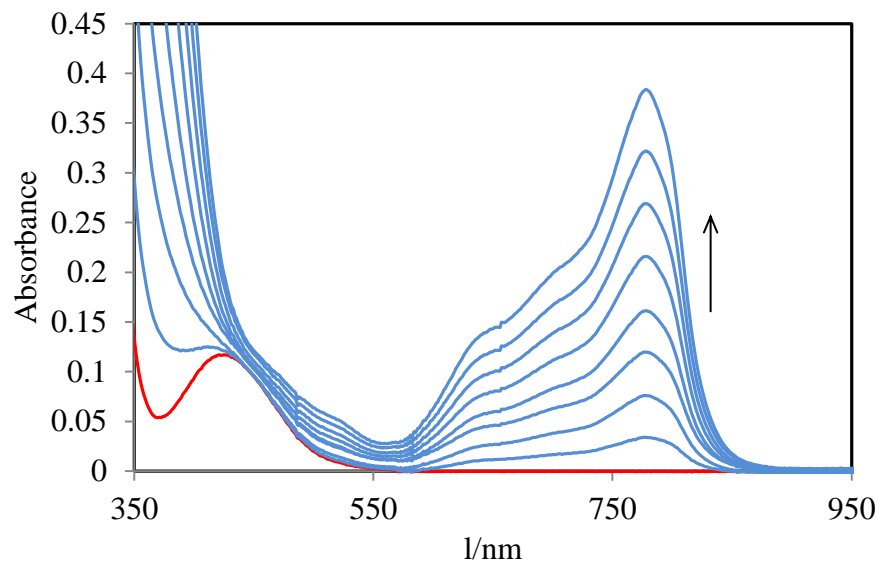


Figure S7. Spectral changes following addition of CBr_4 (150 mM) to the 2 mM Fc^* solution in acetonitrile. Time after mixing (in, blue lines from the bottom to the top at 780 nm): 5, 11, 18, 24, 34, 46, 61, 85 min. Red line represents spectrum of Fc^* .

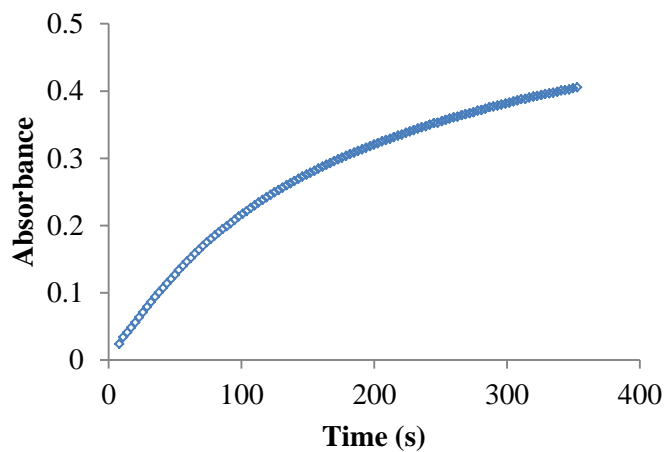


Figure S8. Changes of the intensity of absorbance at 778 nm (corresponding to Fc^{*+}) upon addition of CBr_3NO_2 (0.5 mM) to the 1 mM solution of Fc^* in dichloromethane.

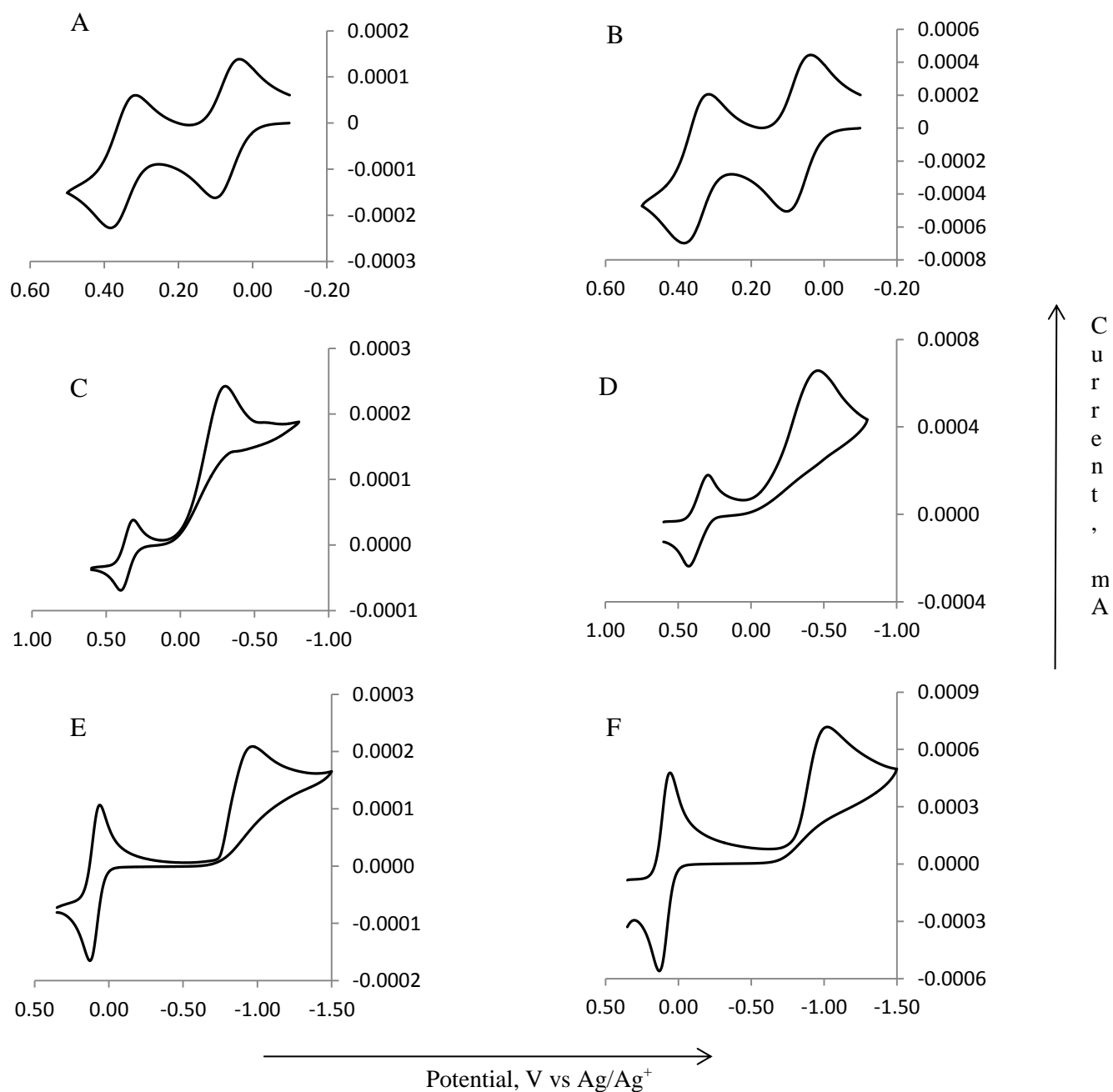
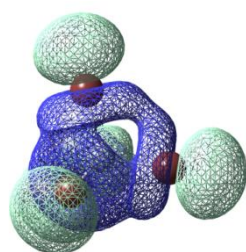
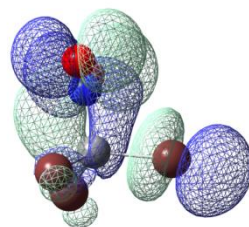


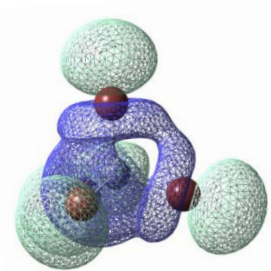
Figure S9. Cyclic voltammograms of TMPD (A and B) CBr₃NO₂ (C and D) and CBr₄ (E and F) measured with Fc⁺/Fc internal standard in acetonitrile (5mM solutions, glassy carbon working electrode, Pt wire auxiliary electrode, Ag/Ag⁺ reference electrode, 0.1 M Bu₄N PF₆ supporting electrolyte measured at 100 mV/s scan rate (A, C, E) and 1000 mV/s (B,D,F).



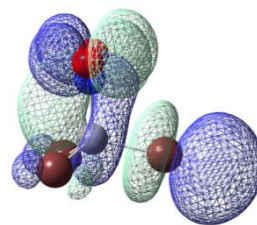
LUMO of CBr_4



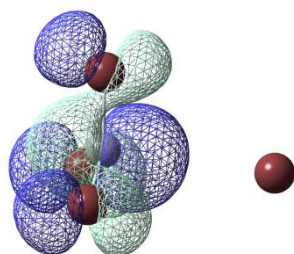
LUMO of CBr_3NO_2



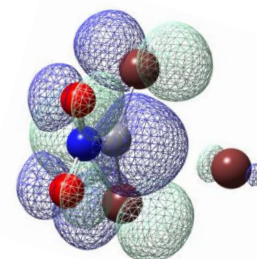
SOMO of $\text{CBr}_4^{\bullet-}$



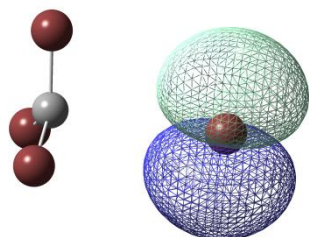
SOMO of $\text{CBr}_3\text{NO}_2^{\bullet-}$



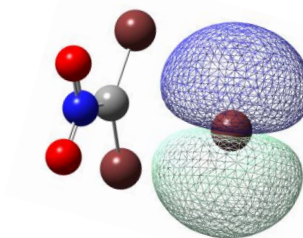
SOMO of $\text{CBr}_3^{\bullet}/\text{Br}^-$



SOMO of $\text{CBr}_2\text{NO}_2^{\bullet}/\text{Br}^-$



HOMO of $\text{CBr}_3^{\bullet}/\text{Br}^-$



HOMO of $\text{CBr}_2\text{NO}_2^{\bullet}/\text{Br}^-$

Figure S10. The shape of LUMOs (top) of neutral CBr_4 and CBr_3NO_2 molecules, SOMOs (middle) of excited anion-radical $\text{CBr}_4^{\bullet-}$ and $\text{CBr}_3\text{NO}_2^{\bullet-}$ (i.e., resulted from “vertical” electron transfer to neutral molecule) as well as SOMOs and HOMOs of final stable $\text{R}^{\bullet}/\text{Br}^-$ products (see coordinates and energies of $\text{R}^{\bullet}/\text{Br}^-$ pairs on p S7). The dark blue and light blue colors represent the opposite phases of the wave functions.

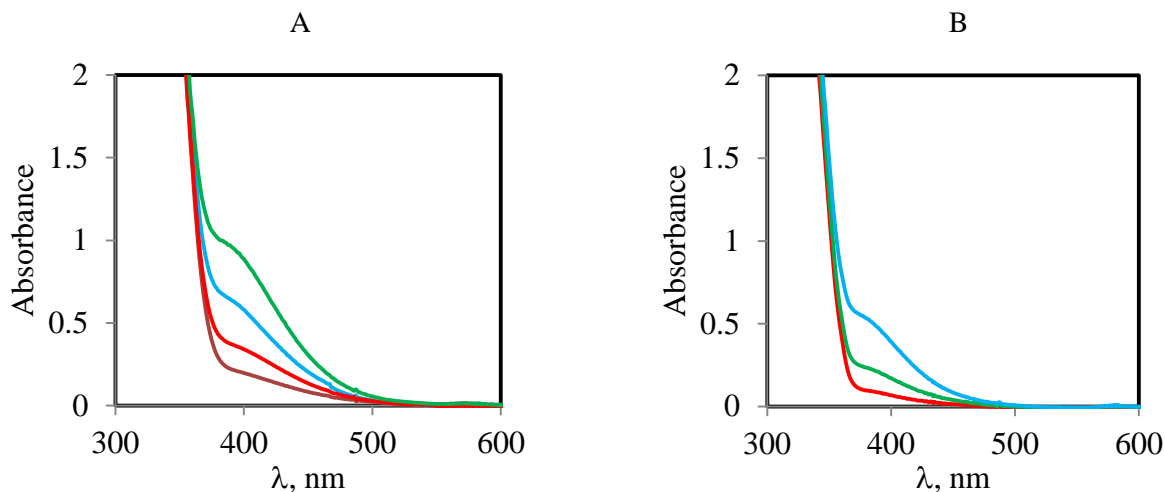


Figure S11. Temperature-dependent spectra of the solutions containing CBr_4 and TMPD (in cuvette with $l = 1$ cm) showing reversible decrease of the absorption band at $\lambda \sim 400$ nm of the $[\text{CBr}_4, \text{TMPD}]$ complex when temperature increases. (Left) 72 mM CBr_4 and 1.4 mM TMPD in CH_2Cl_2 at -54°C (green), -36°C (blue), -20°C (red) and 0°C (brown). (Right) 50 mM CBr_4 and 1.0 mM TMPD in hexane at -48°C (blue), -22°C (green), 3°C (red).

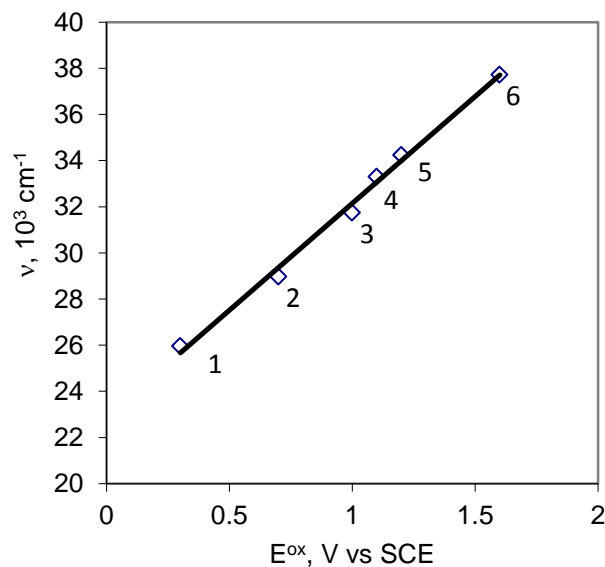


Figure S12. Mulliken dependence of energy of charge-transfer transition vs oxidation potential of donors for series of complexes of CBr_4 acceptor with TMPD (1), I^- (2), SCN^- (3) 9,10-dimethoxy-1,4:5,8-dimethano-1,2,3,4,5,6,7,8-octahydroanthracene (4), Br^- (5) and Cl^- (6) which supports assignment of the absorption band at $\lambda_{\text{max}} = 380$ nm appearing upon addition of TMPD to the solution of CBr_4 (or vice versa) to the $[\text{CBr}_4, \text{TMPD}]$ charge-transfer complex [data from ref. 18].

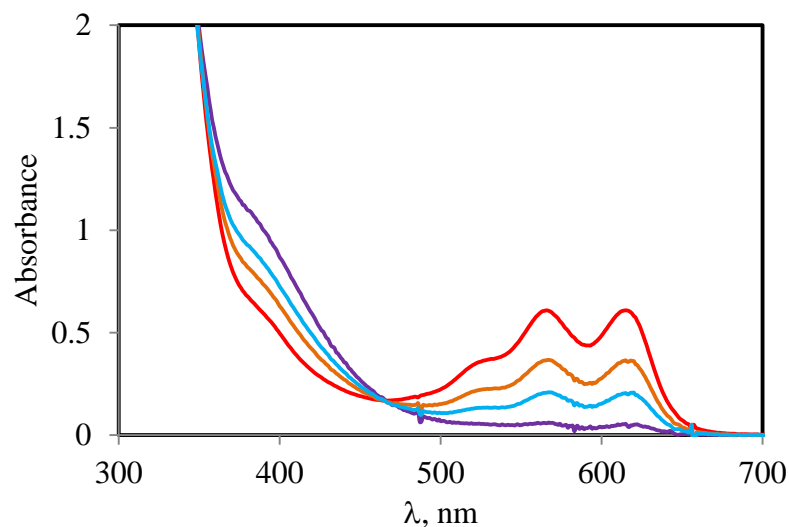


Figure S13. Temperature-dependent spectra of the solution containing 1 mM TMPD and 500 mM CBr_4 in acetonitrile (in cuvette with $l = 1$ cm) showing reversible decrease of the absorption band at $\lambda = 400$ nm of the $[\text{CBr}_4, \text{TMPD}]$ complex accompanied by irreversible formation of $\text{TMPD}^{+\bullet}$ (eq A) as temperature slowly increases from -35°C (violet) to -20°C (blue), -5°C (brown) and 10°C (red)

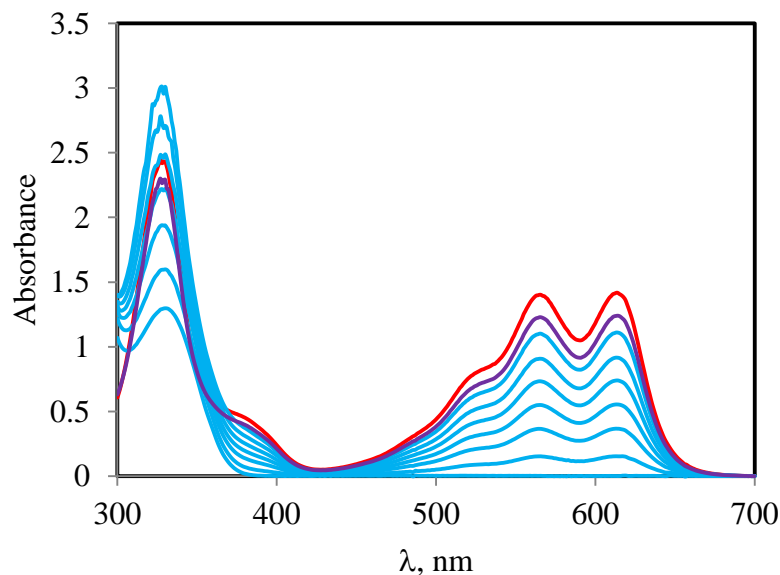
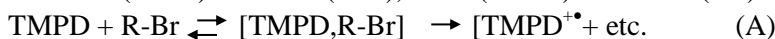


Figure S14. Spectral changes (blue curves) occurring during electrolysis of the TMPD solution in acetonitrile showing formation of $\text{TMPD}^{+\bullet}$ cation radical with $\lambda_{\text{max}} = 619$ nm (electrolysis was carried out on platinum electrode at 0.3 V vs Ag/Ag^+ reference electrode with 0.1 M Bu_4NPF_6 supporting electrolyte). Violet curve represents $\text{TMPD}^{+\bullet}$ cation radical produced by oxidation of TMPD with CBr_3NO_2 and red curve represents 1.2 mM solution of the crystalline salt of $\text{TMPD}^{+\bullet}$ with inert tetrakis[3,5-bis(trifluoromethyl)phenyl]borate anion (which was structurally characterized by single-crystal X-ray measurements in ref. 19).

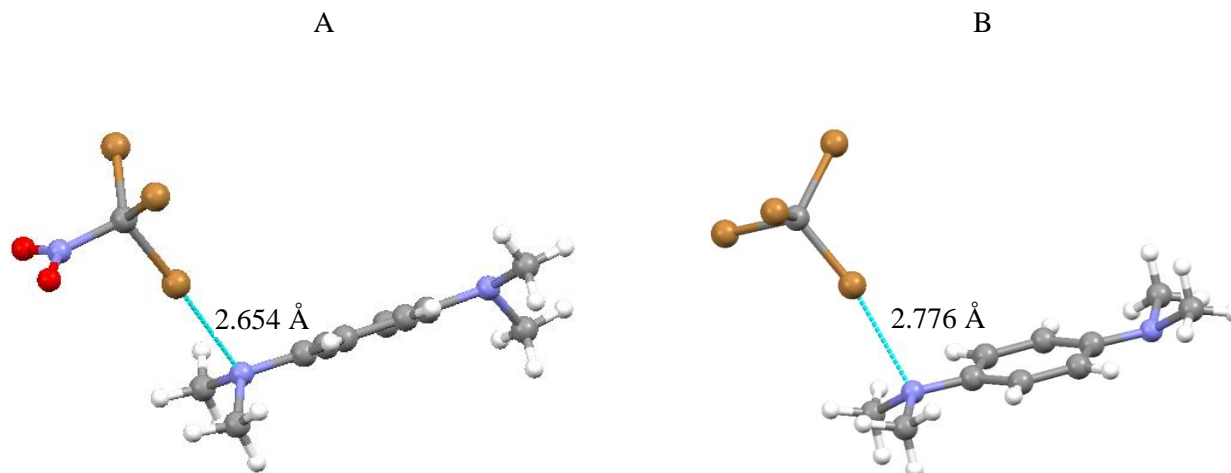


Figure S15. Comparison of halogen bonds (shown as light blue lines) in the experimental (X-ray) structures of $\text{CBr}_3\text{NO}_2/\text{TMPD}$ (measured in the current work) and CBr_4/TMPD (reported in ref. 18).

References

- [1] Heasley, D. R. Titterington, T. L. Rold, G. E. Heasley, *J. Org. Chem.* **1976**, *41*, 1285-7.
- [2] H. A. Benesi, J. H. Hildebrand, *J. Am. Chem. Soc.* **1949**, *71*, 2703-7.
- [3] S. V. Rosokha, C. L. Stern, J.T. Ritzert, *Chem. Eur. J.* **2013**, *19*, 8774-8788.
- [4] S.V. Rosokha, J.K. Kochi, *J. Am. Chem. Soc.*, **2007**, *129*, 828-838.
- [5] See, e.g.: W.B. Pearson, *J. Am. Chem. Soc.*, **1965**, *87*, 167-170.
- [6] (a) R.A. Marcus, N. Sutin, R.A. *Biochim. Biophys. Acta*, **1985**, *811*, 265-322. (b) Marcus, *Angew. Chem. Int. Ed.* **1993**, *32*, 1111-1121.
- [7] See, e.g. T.Nakanishi, K. Ohkubo, T. Kojima, S. Fukuzumi *J. Am. Chem. Soc.*, **2009**, *131*, 577-84.
- [8] (a) A. Cardinale, A. A. Isse, A. Gennaro, M. Robert, J.-M. Saveant, *J. Am. Chem. Soc.* **2002**, *124*, 13533-39. (b) C. Costentin, M. Robert, J.M.Saveant, *Chem. Phys.* **2006**, *324*, 40-56.
- [9] D. Sun, S.V. Rosokha, J. K. Kochi, *J. Phys. Chem. B*, **2007**, *111*, 6655-6666.
- [10] S.V. Rosokha, J.K. Kochi, *J. Am. Chem. Soc.*, **2007**, *129*, 3683-3697.
- [11] T. Gennett, D.F. Milner, M.J. Weaver, *J. Phys. Chem. B*, **1985**, *89*, 2787-2794.
- [12] C. Y. Lin, M. L. Coote, A. Gennaro, K. Matyjaszewski, *J. Am. Chem. Soc.* **2008**, *130*, 12762-74.
- [13] (a) Sutin, N. *Prog. Inorg. Chem.*, **1983**, *30*, 441-498. (b) B.S. Brunshwig, N. Sutin, *Coord. Chem. Revs.* **1999**, *187*, 233 - 254.
- [14] See S.V. Rosokha, M.D. Newton, A.S. Jalilov, J. K. Kochi, *J. Am. Chem. Soc.*, **2008**, *130*, 1944-52 and references therein.

- [15] (a) K.A. Sharp and A. Nicholls, Delphi, v3.0, 1989; See e.g.: (b) K. A. Sharp and B. Honig, *Ann. Rev. Biophys. Chem.* **1990**, *19*, 301. (c) Delphi (designated to solve the Poisson - Boltzman equation) is used here to solve the simpler Poisson equation.
- [16] Gaussian 09, Revision A.1, M. J. Frisch, G. W. Trucks, H. B. Schlegel, G. E. Scuseria, M. A. Robb, J. R. Cheeseman, G. Scalmani, V. Barone, B. Mennucci, G. A. Petersson, H. Nakatsuji, M. Caricato, X. Li, H. P. Hratchian, A. F. Izmaylov, J. Bloino, G. Zheng, J. L. Sonnenberg, M. Hada, M. Ehara, K. Toyota, R. Fukuda, J. Hasegawa, M. Ishida, T. Nakajima, Y. Honda, O. Kitao, H. Nakai, T. Vreven, J. A. Montgomery, Jr., J. E. Peralta, F. Ogliaro, M. Bearpark, J. J. Heyd, E. Brothers, K. N. Kudin, V. N. Staroverov, R. Kobayashi, J. Normand, K. Raghavachari, A. Rendell, J. C. Burant, S. S. Iyengar, J. Tomasi, M. Cossi, N. Rega, J. M. Millam, M. Klene, J. E. Knox, J. B. Cross, V. Bakken, C. Adamo, J. Jaramillo, R. Gomperts, R. E. Stratmann, O. Yazyev, A. J. Austin, R. Cammi, C. Pomelli, J. W. Ochterski, R. L. Martin, K. Morokuma, V. G. Zakrzewski, G. A. Voth, P. Salvador, J. J. Dannenberg, S. Dapprich, A. D. Daniels, O. Farkas, J. B. Foresman, J. V. Ortiz, J. Cioslowski, and D. J. Fox, Gaussian, Inc., Wallingford CT, **2009**.
- [17] A.A. Isse, C. Y. Lin, M. L. Coote, A. Gennaro, *J. Phys. Chem. B*, **2011**, *115*, 678-684.
- [18] S.V. Rosokha, I.S. Neretin, T.Y. Rosokha, J. Hecht and J.K. Kochi, *Heteroat. Chem.* 2006, **17**, 449.
- [19] S. V. Rosokha, C. L. Stern, J.T. Ritzert, *CrystEngComm*. **2013**, DOI:10.1039/C3CE41719.